

Optical Nano-Tomography on Photosensitive Single-Wall Carbon Nanotube Arrays in Zeolite Crystals

Nobukata NAGASAWA^{1,2}, Hirokazu SUGIYAMA¹, Nobuko NAKA^{1*}, Igor KUDRYASHOV³,
Zhao-Ming LI² and Zi-Kang TANG²

¹Department of Physics, Graduate School of Science, The University of Tokyo, 7-3-1 Hongo, Bunkyo-ku, Tokyo 113-0033, Japan

²Department of Physics and Institute of Nano Science and Technology, Hong Kong University of Science and Technology, Kowloon, Hong Kong, China

³Tokyo Instruments, Inc., Nishikasai, Edogawa-Ku, Tokyo 134-0088, Japan

(Received October 3, 2003; accepted October 23, 2003; published February 10, 2004)

Single-wall carbon nanotubes of the smallest diameter formed in microchannel arrays of Zeolite single crystals (IUPAC cord: AFI) have attractive potential for fundamental and device-oriented optical researches. Here we report on very photosensitive characteristics of the material at room temperature. We find that tightly focused irradiation of the 488 nm Ar⁺-ion laser light causes remarkable suppression of the visible emission from nanotubes. The photo-induced suppression occurs under low-level irradiation less than 1 μ W. By the nano-tomography performed with *Nanofinder*, a three-dimensional spectro-tomographic system based on a confocal laser microscope, the size of the affected region is estimated to be 1 μ m \times 1 μ m \times 2 μ m. This is comparable to the effective volume of the photo-irradiation spot. We discuss the origin of the photo-irradiation effects in view of the effects of the thermal conduction along the tube axis and of the local electronic effects within the photo-irradiated region. [DOI: 10.1143/JJAP.43.868]

KEYWORDS: carbon nanotubes, visible emission, photo-induced effect, confocal laser microscope

1. Introduction

Since the discovery of carbon nanotubes, CNs,²⁾ this material has been extensively studied in view of fundamental material science and promising device-oriented researches. Recently, it has been reported that single-wall carbon nanotubes (SWCNs) of 0.4 nm diameter are formed in micro-channel arrays of Zeolite crystals (IUPAC cord: AFI).³⁾ Comparing with widely studied CNs, one of the noticeable characters of the present SWCNs is their small diameter. Three types of SWCNs with different chiralities, (5,0), (4,2) and (3,3), are allowed to be formed in the channels.

Another noticeable character lies in the structure of the AFI crystal. The AFI crystal is a hexagonal prism of AlPO₄-5. The micro-channels align along the *C*-axis and form a hexagonal close-packed array. Therefore, the SWCNs encapsulated in the channels are also aligned. This character makes electrical measurements of the AFI-SWCN system convenient. Since AFI itself is an electrical insulator, all the SWCNs are electrically insulated by the wall of channels. Electrical properties including super-conductive character have been reported in this composite system.⁴⁾ The electrical conduction is considered to be due to the SWCNs encapsulated in the channels.

As an additional noticeable character, we would like to take up optical properties, which have not been studied well so far. The AFI is optically transparent and almost optically isotropic in the region from near infrared to near ultraviolet.⁵⁾ Since interband transitions between valence and conduction bands of the SWCNs are expected to lie in this energy region, one can study relevant optical properties of aligned SWCNs as they are encapsulated in the micro-channel arrays.

CNs can show strong optical anisotropy⁶⁻⁸⁾ reflecting the

quasi one-dimensional structure. Namely, the optical absorption should show its maximum when the electric field vector of incident light, *E*, is parallel to the tube axis. In fact, such polarization anisotropy has been confirmed by absorption spectroscopy of aligning nanotubes dispersed in uniaxially extended organic sheets.⁹⁾ The AFI-SWCN system also shows polarization anisotropy, in an even more sophisticated manner: In this system, the optical absorption really shows remarkable maximum in the *E* \parallel *C* configuration, where *C* is the *C*-axis of the AFI crystal. This anisotropy is considered as direct manifestation of the anisotropic absorption of respective SWCNs aligning without any distribution in orientation.^{10,11)}

On the other hand, we have reported that AFI-SWCN system shows strong visible emission under Ar⁺-ion laser light excitation at 488 nm at room temperature.¹²⁾ AFI crystals themselves show no such strong emission. The intensity of the emission showed maximum under the *E* \parallel *C* configuration, suggesting that the emission is strongly correlated to the optical absorption due to the SWCNs. We have recognized that the spectral shape of the emission depends strongly on the source of samples, locations in respective samples and the condition of the photo-irradiation.¹³⁾

In this paper, we demonstrate three-dimensional diagnostics of the shape and the size of the region where tightly focused photo-irradiation affects the visible emission of SWCNs. A *Nanofinder*,¹⁾ or a three-dimensional spectro-tomographic system based on a confocal laser microscope, which has nano-scale spatial resolution, is used to know the origin of the photo-irradiation effects.

2. Experimental

AFI-SWCN crystals were grown by Tang's group.³⁾ The typical size of the crystals is about 100 μ m wide and 300 μ m long. One side face of the AFI-SWCN crystal was fixed on a slide glass at the edge to keep the sample stress-free during the measurements. A *Nanofinder*¹⁾ (Tokyo Instruments, Inc.)

*Present address: Frontier Research System, RIKEN, 2-1 Hirosawa, Wako, Saitama 351-0198, Japan. E-mail address: n-naka@postman.riken.go.jp

was used for nano-spectroscopy and three-dimensional tomography by the emission from nanotubes. This system is composed of a confocal microscope and a spectrometer with a CCD camera system.¹⁴⁾ A piezo positioner system is installed to scan the location of the observing spot in a sample. We used an objective lens ($\times 100$) of numerical aperture 0.95, and the spatial resolution was 200 nm in x and y directions and 1 μm in z direction. The inset of Fig. 1 shows the schematic illustration of the geometrical configuration of the measurements. The C -axis of the crystal was set parallel to x as shown in the illustration. Ar^+ -ion laser light at 488 nm was introduced into the system by a single mode glass fiber. The sample was irradiated by the laser light on one of side surfaces through the objective lens. The intensity of the incident light for tomography was reduced as possible to avoid photo-irradiation effects. The spectral shapes were corrected by the transmission spectrum of *Nanofinder*, estimated with a calibrated Halogen lamp (Oriel, 63355).

3. Results and Discussion

Figure 1 shows typical emission spectra of the AFI-SWCN system in polarization configurations of (a) $E \parallel C$ and (b) $E \perp C$, respectively. The arrow shows the wavelength of the laser light. The intensity of emission showed its maximum in $E \parallel C$ geometry corresponding to the polarization anisotropy observed in the absorption spectra.¹¹⁾ The present visibility is estimated to be about 0.85.

One of the authors, H. Sugiyama, has found¹⁵⁾ that the

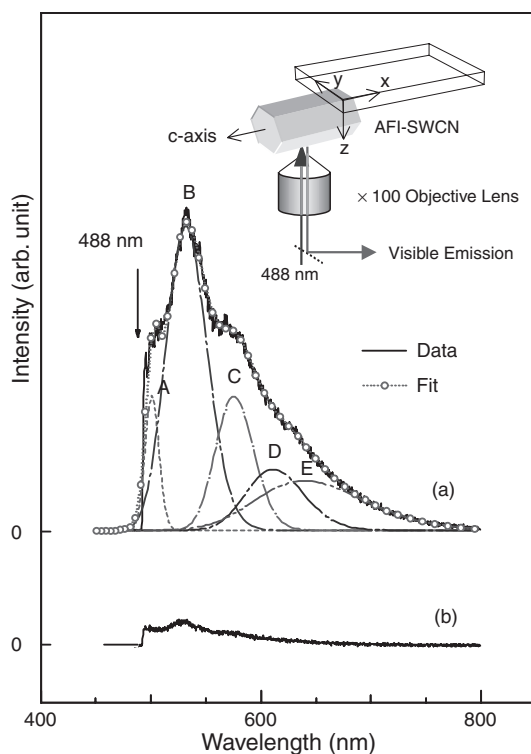


Fig. 1. Emission spectra under 488 nm Ar^+ -ion laser light irradiation in polarization configurations of (a) $E \parallel C$ and (b) $E \perp C$. Solid curves show measured spectra and the dotted curve with circles shows the fitting result of the superposition of five Gaussian components. Respective components are also shown by dashed and dash-dotted lines. The inset shows the schematic illustration of the experimental configuration.

spectral shape is reproduced completely as a superposition of a set of Gaussian components of different intensities, even if spectral shapes are seemingly different. As shown in the figure, the spectrum can be decomposed into five Gaussian bands peaked at 500, 520, 570, 610, and 650 nm. They are named as A, B, C, D and E, respectively. We have found that peak energies of A and B, measured from the excitation photon energy, almost correspond to the energies of Radial Breathing (534 cm^{-1}) and Tangential Graphite ($1550\text{--}1600 \text{ cm}^{-1}$) modes of SWCNs, respectively.¹⁶⁾ We concluded, therefore, that the origin of the emission correlates with the SWCNs. No corresponding Raman lines were observed because of low-level excitation.

Figure 2(a) shows the intensity distribution of the emission on the xy plane near the surface of the sample in the $E \parallel C$ configuration. We took this data before testing the photo-irradiation effects, by integrating the emission in the wavelength region between 496 nm and 700 nm. The excitation intensity was $0.5 \mu\text{W}$. The scanning time to cover all the xy space was set for 80 s. Then, the excitation spot moves at a speed of 20 nm/ms. As seen in the figure, the emission intensity was not homogeneous. The spectral shape, however, was almost identical within this scanning region. P and Q pointed by arrows indicate the locations selected to test photo-irradiation effects. The polarization configuration of the photo-irradiation was $E \parallel C$ at P and $E \perp C$ at Q, with the same excitation density of $1.5 \mu\text{W}$ for 1 min. After the photo-irradiation at respective locations, the intensity distribution of the emission was measured once again at $0.5 \mu\text{W}$ in the $E \parallel C$ configuration.

Curves shown in Fig. 2(b) are the emission spectra at P before and after the photo-irradiation. The spectral shape was unchanged but the intensity was reduced remarkably. Figure 2(c) shows the distribution of the difference in intensities between before and after the photo-irradiation. Irradiated regions are clearly seen as dark spots at P and Q. The shape of each printed spot was almost circle.

In the figure, horizontal dark lines and a vertical dark band are seen. The origin of the horizontal lines is due to the incomplete subtraction of images obtained before and after the photo-irradiation. On the other hand, the origin of the vertical dark band is the trace of scanning on the yz plane through Q, preliminary tried before the measurement. This shows that the photo-irradiation effects occur very efficiently.

Figure 2(d) shows the intensities of emission along the horizontal line through P (solid line) and Q (dashed line). The depth at P is about two times larger than that at Q. The difference reflects the different absorption coefficients for $E \parallel C$ and $E \perp C$ configurations. The second dip for the solid line at Q is due to the effect of the pre-scanning mentioned above.

Figure 3 shows the intensity distributions on the xz plane through P, (a) before and (b) after the photo-irradiation. Figure 3(c) was obtained by the pixel subtraction between the pattern of (b) and that of (a). The pattern on the xy plane through P was similar to that in Fig. 3(c). The curves in Figs. 3(d) and 3(e) show the intensity distributions in x and z cross-sections through P, as marked by dashed lines labeled (i) and (ii) in Fig. 3(c).

The shape of the photo-modulated region provides

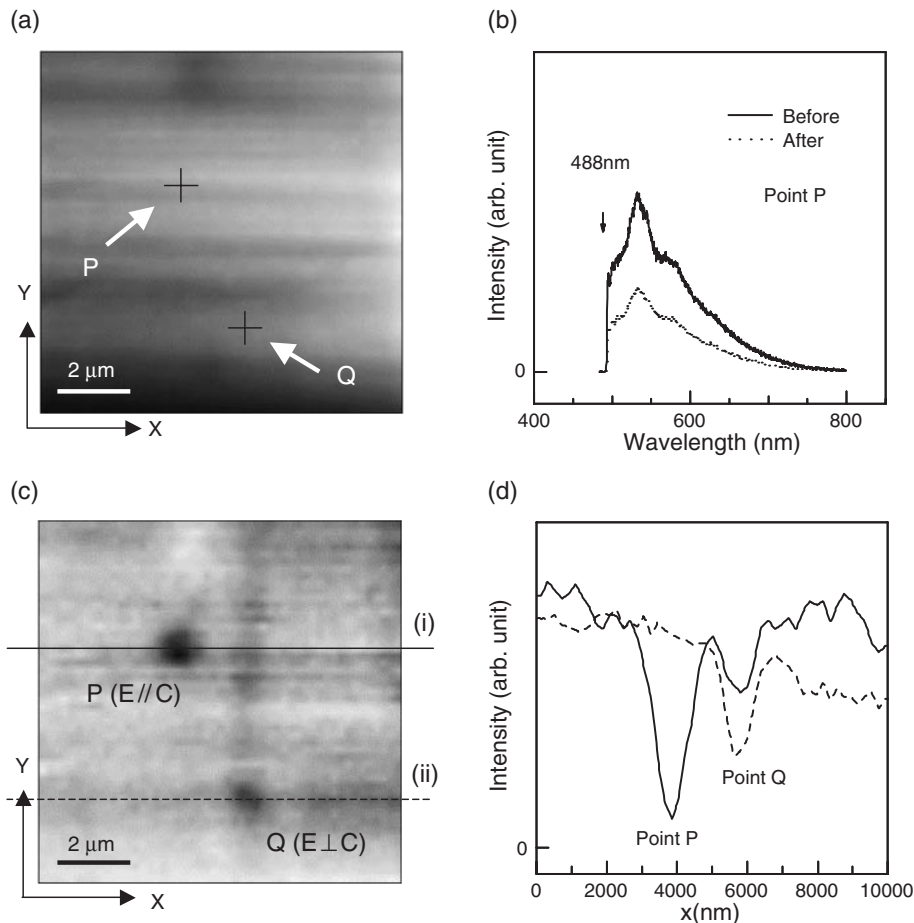


Fig. 2. Spatial feature of the photo-irradiation effects. (a) Intensity distribution of emission integrated in the wavelength region between 496 nm and 700 nm on the xy plane in the $E \parallel C$ configuration. P and Q indicate the locations selected to test photo-irradiation effects under $E \parallel C$ and $E \perp C$ configurations, respectively. (b) Emission spectra at P before and after the photo-irradiation; (c) distribution of the difference in intensities between before and after photo-irradiation; (d) emission intensities as a function of x through P (solid line) and Q (dashed line).

information about the origin of the photo-irradiation effects or photo-induced suppression of the emission. We shall discuss two origins compatible with our observations that the spatial pattern of the photo-modulated region is almost circular on the xy plane.

One is thermal effect caused by the photo-irradiation in the absorption region. After the electronic excitation, the excited electrons relax to generate heat. Since Zeolite works as good thermal insulator, respective tubes within the excited volume should be heated homogeneously along the tube axis reflecting the large thermal conductivity.¹⁷⁾ If this process is dominant, the spatial pattern of the photo-modulated region on the xy plane should be anisotropically expanded along the tube axis that is parallel to the x -axis. However, this is not the case of our observation. Generally, thermal conductivity depends on the density of defects in tubes. If the isotropic shape on the xy plane is due to the decrease of the thermal conductivity due to defects, the origin of the photo-induced suppression would be due to local heating caused by the photo-irradiation. The shape along z direction was also limited within the effective excitation volume. This suggests that effects of heat conduction through Zeolite do not contribute remarkably to the suppression of the emission as expected.

Another one is of electronic origin: If photo-excited electrons can move quickly along the tube axis, the photo-excited carriers that cause the photo-induced suppression should homogeneously distribute in a tube. Assuming that respective tubes are electronically isolated each other, the shape should be also anisotropically expanded along the tube axis. To realize the isotropic distribution on xy plane, the excited carriers should be trapped quickly by self-trapping or some defects. More study is necessary to identify the reason of the trapping.

In this paper, we have only discussed the photo-induced suppression observed in the lowest irradiation power. According to our preliminary experiments in a higher irradiation regime, anisotropy in the photo-modulated region has been observed on the xy plane. In this case, we suppose that the origin is thermal effects discussed above. In such a high irradiation regime, the spectral shape of emission also showed remarkable change. Further systematic study in a high-density excitation regime seems promising. On the other hand, we have reported photo-modulation of I - V characteristics of similar AFI-SWCNs showing metallic conduction.¹⁸⁾ The correlated studies on photo-modulation in emission and electric conduction are desired. The experiments along this line are in progress.

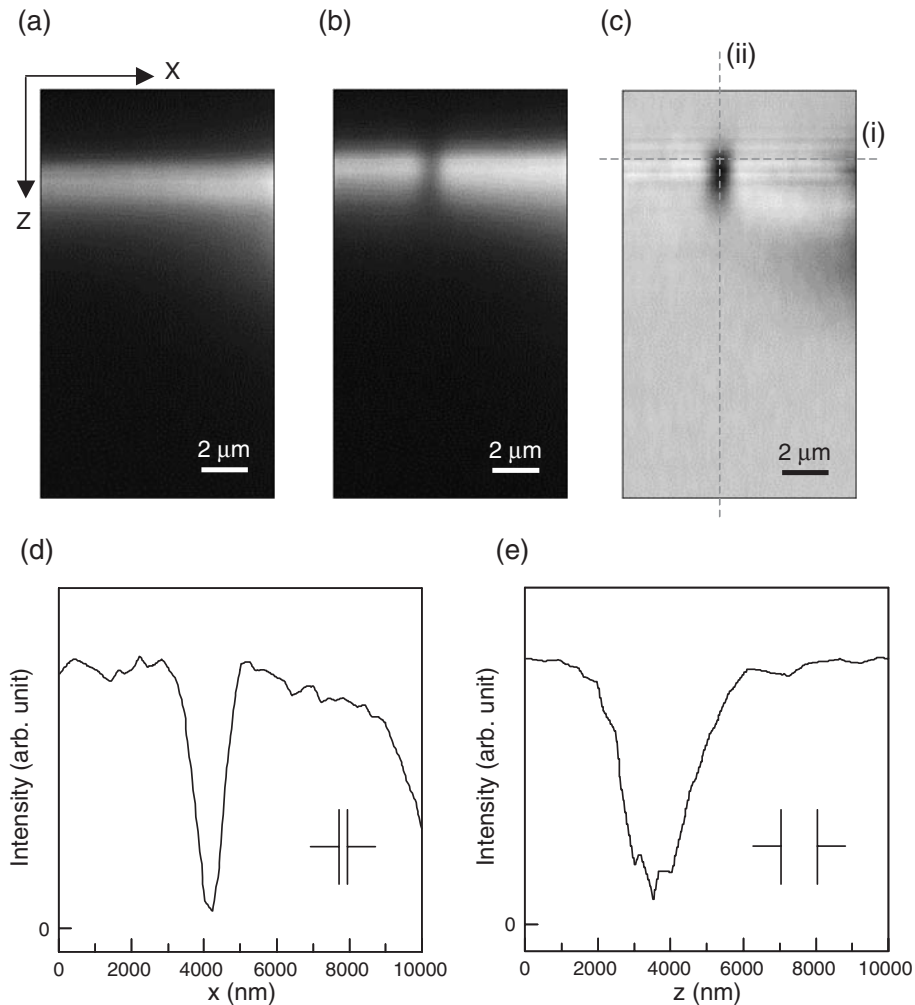


Fig. 3. Spatial feature of photo-irradiation effects. (a) and (b) Intensity distributions before and after the photo-irradiation on the xz plane at P. (c) Pixel subtraction of the pattern of (b) from that of (a). (d) Emission intensity as a function of x along dashed line (i) shown in (c). (e) Emission intensity as a function of z along dashed line (ii) shown in (c).

4. Conclusions

Nano-tomographic spectroscopy was performed by using a *Nanofinder* to measure the spatial distribution of photo-induced suppression of visible emission from the AFI-SWCN system at room temperature. The suppression occurred effectively in a very low excitation level and was dominant in the $E \parallel C$ configuration. These are correlated to the polarization anisotropy of the corresponding optical absorption. The origin of the photo-irradiation effects was discussed on the basis of their isotropic geometrical features.

Acknowledgments

One of the authors (N. Nagasawa) would like to thank Mr. S. Suruga (Tokyo Instruments, Inc.) for his support to this collaboration research. This work was partially supported by The Mitsubishi Foundation for Scientific Research and RGC and DAG grants of Hong Kong.

- 1) *Nanofinder* is a registered trademark of Tokyo Instruments, Inc.
- 2) S. Iijima: *Nature* **354** (1991) 56.
- 3) N. Wang, Z. K. Tang, G. D. Li and J. S. Chen: *Nature* **408** (2000) 50.
- 4) Z. K. Tang, L. Y. Zhang, N. Wang, X. X. Zhang, G. H. Wen, G. D. Li, J. N. Wang, C. T. Chan and P. Sheng: *Science* **292** (2001) 2462.

- 5) K. Hoffmann, F. Marlow and J. Caro: *Zeolites* **16** (1996) 281.
- 6) H. Ajiki and T. Ando: *Physica B* **201** (1994) 349.
- 7) S. Tasaki, K. Maekawa and T. Yamabe: *Phys. Rev. B* **57** (1998) 9301.
- 8) I. Bozovic, N. Bozovic and M. Damnjanovic: *Phys. Rev. B* **62** (2000) 6971.
- 9) M. Ichida, S. Mizuno, H. Kataura, Y. Achiba and A. Nakamura: *AIP Conf. Proc.* **590** (2001) 121.
- 10) Z. K. Tang, Z. M. Li, G. D. Li, N. Wang, H. J. Liu and C. T. Chan: *AIP Conf. Proc.* **590** (2001) 125.
- 11) Z. M. Li, H. J. Liu, N. Wang, C. T. Chan, R. Saito, S. Okada, G. D. Li, J. S. Chen, N. Nagasawa and S. Tsuda: *Phys. Rev. Lett.* **87** (2001) 127401.
- 12) N. Nagasawa, I. Kudryashov, S. Tsuda and Z. K. Tang: *AIP Conf. Proc.* **590** (2001) 213.
- 13) N. Nagasawa, H. Sugiyama, N. Naka, I. Kudryashov, M. Watanabe, T. Hayashi, I. Bozovic, N. Bozovic, G. Li, Z. Li and Z. K. Tang: *J. Lumin.* **97** (2002) 161.
- 14) I. Kudryashov, P. Rutkovski and S. Suruga: *Lecture Summary Book of 2002, Spring Conference Research Group Symposium: Frontline of micro-vibrational spectroscopy, 2002*, p. 47.
- 15) H. Sugiyama: *Master Thesis, University of Tokyo, 2002*.
- 16) A. Jorio, A. G. Souza, G. Dresselhaus, M. S. Dresselhaus, A. Righi, F. M. Matinaga, M. S. S. Dantas, M. A. Pimenta, J. Mendes, Z. M. Li, Z. K. Tang and R. Saito: *Chem. Phys. Lett.* **351** (2002) 27.
- 17) S. Berber, Y. K. Kwon and D. Tomanek: *Phys. Rev. Lett.* **84** (2000) 4613.
- 18) Y. Kamada, N. Naka, S. Saito, N. Nagasawa, Z. M. Li and Z. K. Tang: *Solid State Commun.* **123** (2002) 375.